Quantum enhanced imaging of nonuniform refractive profiles

(Article begins on next page)

19 May 2022

World Scientific
www.worldscientific.com

Quantum enhanced imaging of nonuniform refractive profiles

Giuseppe Ortolano*,†,§, Ivano Ruo-Berchera* and Enrico Predazzi‡

*Quantum Metrology and Nano Technologies Division,
INRiM - Istituto Nazionale di Ricerca Metrologica,
Strada Delle Cacce 91, 10135 Torino, Italy

†DISAT - Dipartimento Scienza Applicata e Tecnologia,
Politecnico di Torino, Corso Duca Degli Abruzzi 24,
10129 Torino, Italy

‡Dipartimento di Fisica - Universita di Torino
and Sezione INFN di Torino-Via P. Giuria 1, Torino, Italy
§giuseppe.ortolano@polito.it

In this work, quantum metrology techniques are applied to the imaging of objects with a nonuniform refractive spatial profile. A sensible improvement on the classical accuracy is shown to be found when the "Twin Beam (TWB) State" is used. In particular, exploiting the multi-mode spatial correlation, naturally produced in the Parametric Down Conversion (PDC) process, allows a 2D reconstruction of complex spatial profiles, thus enabling an enhanced imaging. The idea is to use one of the spatially multimode beams to probe the sample and the other as a reference to reduce the noise. A similar model can also be used to describe wave front distortion measurements. The model is meant to be followed by a first experimental demonstration of such enhanced measurement scheme.

Keywords: Quantum imaging; non-classical correlations; gradient-index.

1. Introduction

In recent years, quantum states of light have been proven successful in the enhancement of a variety of measurement schemes,[1,2] such as undetected photon imaging,[3] quantum illumination,[4–6] super resolution,[7,8] ghost imaging,[9–14] interferometry[15–18] and absorption imaging.[2,19–21] In particular, a fundamental limit in the accuracy of classical schemes is the Shot Noise Limit (SNL),[22,23] that bounds the uncertainty in the estimation of a parameter to scale as the inverse square root of

G. Ortolano, I. Ruo-Berchera & E. Predazzi

the photons involved. Schemes that enable to surpass the SNL are of paramount importance in settings, where the energy that can be used is limited, as it is the case, for example, when dealing with biological samples[24] that could be damaged by the radiation. Sub-SNL measurements have been realized, using squeezed states of light for interferometry,[25,26] beam displacement measurements,[27–29] particle tracking in living systems[30] and recently sub-SNL wide field absorption imaging has been achieved[20,31,32] using quantum correlated states. A state often used in such schemes is the Twin Beam (TWB) state produced by the process of Parametric Down Conversion (PDC)[33,34] or four-wave mixing.[35,36] In PDC, a laser pump interacts with a nonlinear crystal creating, as a result, a pair of photons correlated both in position and momentum. This state is particularly interesting not only because the use of quantum correlations allows a reduction of the uncertainty of an estimation below the SNL, but also because of the spatial multimode nature of the PDC process, that automatically enables wide field imaging, meaning that a 2D spatial profile can be imaged with a single exposure.[32] It can be expected that the TWB state, similarly as it is in the case of absorption imaging, can be used to achieve sub-SNL measurements of nonuniform refractive profiles and aim of this work is, in fact, to investigate the improvements that the use of quantum correlations would bring to such measurements. Classically, different techniques are used to image a non uniform refractive profile of an object. Considering a beam interacting with the object, a deflection of a certain angle is produced, that can be analyzed using ray optics[37] under suitable assumptions, depending on the scheme considered. In particular, the Schilieren configuration[38] focuses on the imaging of the gradient of the refractive profile ∇n while in shadography[38] the image formed is proportional to $\nabla^2 n$. A common point for those kind of schemes is that for each point of the object, the angle of deflection containing information on the refractive profile is retrieved by measuring the change in the intensity distribution at the detection plane, by means of a multipixel detector.
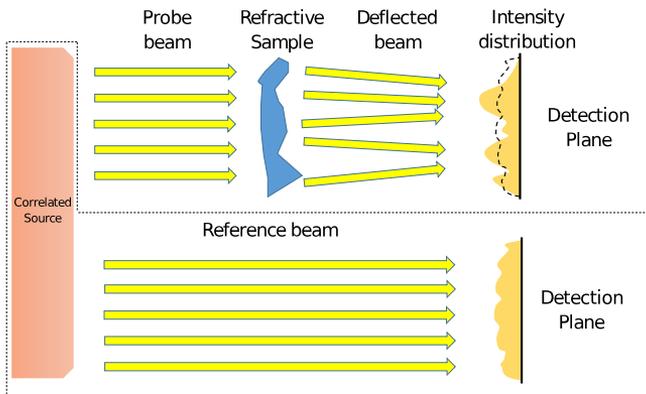

Fig. 1. *Wide field imaging of a refractive profile.* A sample is illuminated by a spatial multimode beam. At each position the beam is deflected at a different angle, altering the intensity distribution. In the dashed shape the configuration in which the beam is correlated to another, used as reference, is pictured.

In this paper we analyze the possible quantum advantage achievable in a scheme where, similarly, the deflection is estimated by a measurement of the intensity distribution, so that the uncertainty of the estimation depends on the statistics of the detected photons. This problem is similar to the beam displacement problem analyzed in Ref. 28 where the entire beam is deflected of a certain angle and it is detected by a quadrant detector. The difference is that the structure causing the deflection in our case is more complex, in the sense that at each position of the sample incoming light is deflected at a different angle, or no angle at all, as pictured in Fig. 1. The object is considered to be illuminated by a spatially incoherent source with a certain pattern, e.g. the TWB state. The results, after the interaction, are a measured intensity distribution where deflected and nondeflected parts of the probe pattern sum up in intensity at each pixels. Interference effects are not considered here given the incoherent properties of the multimode source.

2. The Model

The analysis of the interaction of the beam with the object can be carried out from a phenomenological point of view as depicted in Fig. 2(a).

In the simplified scheme pictured a single mode, labeled $\hat{a}$ goes through a region with nonuniform refractive index, called an impurity, and, as a result, is deflected downwards of an angle α. In turn, at the detection plane close to the object, photons will be detected in a shifted position. The detectors are positioned such that the one labeled "1" intercepts the first mode, when unperturbed, while an adjacent detector of the same size, labeled "2", receives photons only when there is a deflection. The deflection is assumed small enough that the beam never exceeds the position of detector 2 at detection. In Fig. 2(b) a second mode, labeled $\hat{b}$ and considered independent from the first mode, is added, so that detector 2 in this case collects photons from $\hat{b}$ but also part of the photons from $\hat{a}$ due to the deflection. This last configuration mimics the situation one have in wide field imaging where the object can be
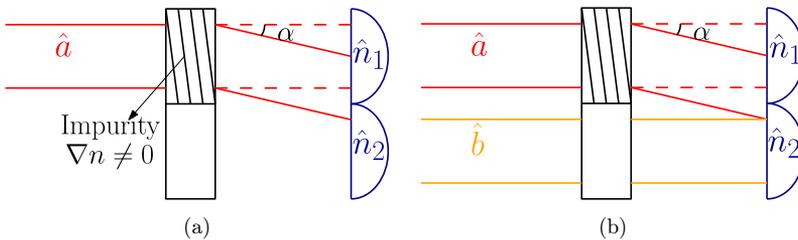

Fig. 2. (a) *Deflection of a single mode due to an impurity*. A single mode, labeled $\hat{a}$, interacts with a test object with a gradient in the refractive index ∇n. As a result $\hat{a}$ is deflected of an angle α. In turn this deflection will cause a shift in the detected position of the photons. (b) *Deflected mode with disturbance*. The difference with the previous scheme is the presence of a second mode, labeled as $\hat{b}$, and considered independent from $\hat{a}$. Due to the deflection some photons from $\hat{a}$ will be detected in the same position as photons from $\hat{b}$.
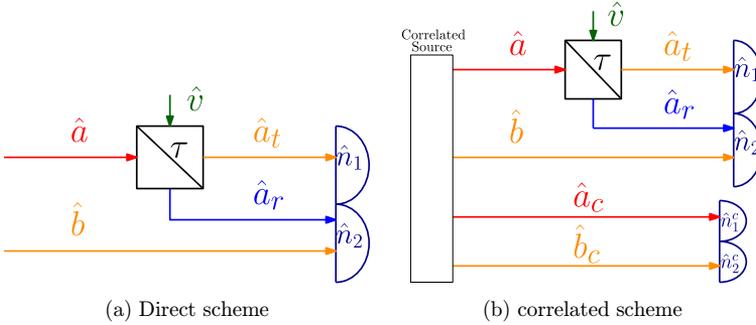
Fig. 3. (a) *Model of beam deflection.* Schematic representation of the situation of Fig. 2(b). The deflection of the beam is modeled with a BS of transmission $0 \leq \tau \leq 1$, where $1 - \tau$ is proportional to the angle of deflection α. (b) *Correlated scheme.* The scheme pictures a deflection measurement. A correlate source is used to produce pairs of correlated modes, $\hat{a}$ correlated to $\hat{a}_c$ and $\hat{b}$ to $\hat{b}_c$. $\hat{a}$ and $\hat{b}$ probe the object, while their respective correlated modes are used as reference.

illuminated simultaneously by different modes at different positions. The following analysis refers to this elementary scheme, but it can be generalized to the situation in which a gradient is present all across the object, producing local deflections.

We develop a quantum statistical model in which the deflection in Fig. 2(b) is represented as the result of a beam splitter (BS) acting on the mode $\hat{a}$ as showed in Fig. 3(a). The BS is characterized by its transmission coefficient τ, the fraction of transmitted photons. The angle of deflection is then proportional to the reflectance $1 - \tau$ where the constant of proportionality depends on the particular spatial distribution of the mode. Estimating the angle of deflection of Fig. 2.B is then equivalent to the estimation of the coefficient τ in Scheme 3(a).

2.1. *Direct scheme and SNL*

Referring to the configuration of Fig. 3(a) the estimation of τ can be carried out using the estimator $\hat{E}$

$$\hat{E} = \frac{\hat{n}_1 - \hat{n}_2}{\hat{n}_1 + \hat{n}_2}, \tag{1}$$

where $\hat{n}_1$ and $\hat{n}_2$ are the photon number operators detected from detectors 1 and 2, respectively. The choice of this estimator, where the role of the denominator is to attenuate the fluctuations, follows from the fact that it allows, under the condition of small photon number fluctuations w.r.t. mean value, to reach the Ultimate Quantum Limit, derived in Ref. 39, in the estimation of a BS parameter with a single input beam, when the second mode $\hat{b}$ is not considered.[40] The estimator $\hat{E}$ is defined using a ratio of operators and his mean value can be found expanding Eq. (1), for small fluctuations around the operator mean value, that at the zeroth order is

$$\langle \hat{E} \rangle = \left\langle \frac{\hat{n}_1 - \hat{n}_2}{\hat{n}_1 + \hat{n}_2} \right\rangle \approx \frac{\langle \hat{n}_1 \rangle - \langle \hat{n}_2 \rangle}{\langle \hat{n}_1 \rangle + \langle \hat{n}_2 \rangle} = \frac{(2\tau - 1)N_a - N_b}{N_a + N_b}, \tag{2}$$

where $N_a = \langle \hat{n}_a \rangle = \langle \hat{a}^\dagger \hat{a} \rangle$ and $N_b = \langle \hat{n}_b \rangle = \langle \hat{b}^\dagger \hat{b} \rangle$ are the mean number of photons in modes $\hat{a}$ and $\hat{b}$. All the mean values $\langle \cdot \rangle$ are taken on the initial state of the field, $\rho_a \otimes \rho_b$. Those states will be specified by means of their photons statistics, and given the physical configuration under analysis, from now on, we will consider ρ_a and ρ_b equal, as the two modes are produced by the same source. An estimation of τ can be found solving Eq. (2), using the fact that N_a and N_b can be considered parameters as they can be determined with arbitrary accuracy in a preliminary characterization of the experimental apparatus, in absence of the sample under test.

The variance $\langle \Delta^2 \hat{E} \rangle$ can be obtained with the propagation of the uncertainty on $\hat{n}_1$ and $\hat{n}_2$ and expressed in terms of the statistic of the input modes $\hat{a}$ and $\hat{b}$.

From the well-known BS relations $\hat{a}_t = \sqrt{\tau}\hat{a} + i\sqrt{(1-\tau)}\hat{v}$ and $\hat{a}_r = i\sqrt{(1-\tau)}\hat{a} + \sqrt{\tau}\hat{v}$, the statistic of the transmitted and reflected modes $\hat{a}_t$ and $\hat{a}_r$ is easily found to be

$$
\begin{aligned}
\langle \hat{n}_t \rangle &= \langle \hat{a}_t^\dagger \hat{a}_t \rangle = \tau N_a, & \langle \hat{n}_r \rangle &= \langle \hat{a}_r^\dagger \hat{a}_r \rangle = (1-\tau)N_a, \\
\langle \Delta^2 \hat{n}_t \rangle &= \tau N_a(\tau F + 1 - \tau), & \langle \Delta^2 \hat{n}_r \rangle &= N_a(1-\tau)(F(1-\tau)+\tau), \\
\langle \Delta \hat{n}_t \Delta \hat{n}_r \rangle &= \tau(1-\tau)N_a(F-1),
\end{aligned}
\tag{3}
$$

The Fano factor[41] $F = \langle \Delta^2 \hat{n} \rangle / \langle \hat{n} \rangle$ was introduced to characterize the statistic of the input state. States with $F < 1$, i.e. characterized by sub-Poissonian fluctuation, are considered nonclassical states of light.[42] The statistic of $\hat{n}_1$ follows directly from relation in Eq. (3) since from scheme in Fig. 3(a) it coincides with $\hat{n}_t$. To determine the statistic of $\hat{n}_2$, we use the fact that $\hat{a}$ and $\hat{b}$ are independent so that we have

$$
\begin{aligned}
\langle \hat{n}_2 \rangle &= \langle \hat{n}_b \rangle + \langle \hat{n}_r \rangle, \\
\langle \Delta \hat{n}_1 \Delta \hat{n}_2 \rangle &= \langle \Delta \hat{n}_t \Delta \hat{n}_r \rangle, \\
\langle \Delta^2 \hat{n}_2 \rangle &= \langle \Delta^2 \hat{n}_b \rangle + \langle \Delta^2 \hat{n}_r \rangle.
\end{aligned}
\tag{4}
$$

So that for $\hat{n}_2$, we get

$$
\begin{aligned}
\langle \hat{n}_2 \rangle &= N_b + (1-\tau)N_a, \\
\langle \Delta^2 \hat{n}_2 \rangle &= FN_b + (1-\tau)^2 FN_a + \tau(1-\tau)N_a, \\
\langle \Delta \hat{n}_1 \Delta \hat{n}_2 \rangle &= \tau(1-\tau)(FN_a - N_a).
\end{aligned}
\tag{5}
$$

Using Eqs. (3) and (5), we can propagate the uncertainty from Eq. (1). Assuming $N_a = N_b = N$, we have

$$
\langle \Delta^2 \hat{E} \rangle \approx \frac{F\tau^2}{2N} + \frac{\tau(1-\tau)}{N}.
\tag{6}
$$

This uncertainty can be propagated to the parameter τ as

$$
\Delta\tau = \frac{\sqrt{\langle \Delta^2 \hat{E} \rangle}}{|\partial \langle \hat{E} \rangle / \partial \tau|}.
\tag{7}
$$

So that

$$\Delta\tau = \sqrt{\frac{F\tau^2}{2N} + \frac{\tau(1-\tau)}{N}}. \tag{8}$$

The minimum fluctuation that can be achieved with "classical" states is the one obtained with coherent states, with $F = 1$, setting the SNL for this scheme:

$$\Delta\tau_{\text{SNL}} = \sqrt{\frac{\tau^2}{2N} + \frac{\tau(1-\tau)}{N}}. \tag{9}$$

2.2. *Correlation based scheme*

In order to take advantage of quantum correlations, we propose another scheme, depicted in Fig. 3(b). A source is used to produce spatially separated pairs of correlated modes. In Fig. 3(b), the modes testing the object, $\hat{a}$ and $\hat{b}$, are correlated to the modes $\hat{a}_c$ and $\hat{b}_c$, respectively, that act as a reference. The aim of this scheme is to exploit correlations in the photon number to improve the accuracy over the direct scheme. The degree of correlation, for a pair of generic modes $\hat{i}$ and $\hat{j}$, is expressed by the noise reduction factor[31]σ defined as

$$\sigma = \frac{\langle\Delta^2(\hat{n}_i - \hat{n}_j)\rangle}{\langle\hat{n}_i + \hat{n}_j\rangle}. \tag{10}$$

With this configuration, the parameter τ can be computed using the estimator $\hat{E}_C$:

$$\hat{E}_C = \frac{\hat{n}_1 - (\hat{n}_2 - \hat{n}_2^c)}{\hat{n}_1^c}. \tag{11}$$

The choice of this estimator is arbitrary but motivated by the fact that the correlation of $\hat{n}_2$ and $\hat{n}_2^c$ should allow to reduce the fluctuation of the bracket term at the numerator, meanwhile normalizing by $\hat{n}_1^c$ compensates for the fluctuation of $\hat{n}_1$.

For small fluctuations in photon numbers, the mean value can be approximated, as done before as

$$\langle\hat{E}_C\rangle \approx \frac{\langle\hat{n}_1 - (\hat{n}_2 - \hat{n}_2^c)\rangle}{\langle\hat{n}_1^c\rangle} = 2\tau - 1. \tag{12}$$

Where $N_a^c = N_a = N_b = N_b^c$ was assumed, which is true for photons in the TWB state if balanced losses are considered. The calculation of the uncertainty is similar to the one showed in Sec. 2.2 and will not be reported. The result is

$$\Delta\tau_C = \sqrt{\frac{\tau(1-\tau)}{N} + \frac{(2\tau-1)^2\sigma}{4N} + \frac{\sigma}{2N}}, \tag{13}$$

that depends only on the measured mean number of photons N in the reference beam and on the measured noise reduction factor in absence of the sample's perturbation.

3. Results and Discussion

From Eqs. (9) and (13), a comparison of the performance in the estimation with different input states can be made. In particular, for the direct scheme of Sec. 2.1, we consider each mode of the multimode beam to be, alternatively, in one of the following states

- The *Fock state*, eigenstate of the photon number operator of the field so that $F_{\text{Fock}} = 0$
- The *coherent state*, eigenstate of the annihilation operator with a Poissonian photon number distribution, hence $F_{\text{coh}} = 1$
- The *thermal state*, a mixed state characterized by the Bose–Einstein distribution at thermal equilibrium, $P(n) = N^n/(1 + N)^{(n+1)}$,[43] having then $F_{\text{th}} = 1 + N$, N being the main number of photons.

The correlation based scheme will be analyzed in the case of the TWB *state*

$$|\psi\rangle_{\text{TWB}} = \sum_n c(n)|n\rangle_{\mathbf{k}_t,\omega}|n\rangle_{-\mathbf{k}_t,-\omega}, \tag{14}$$

where $\mathbf{k}_t$ and ω are the transverse momentum and frequency of the mode and $|c(n)|^2$ is a thermal like distribution. From (14), it is clear that the quantum nature of the state resides in its entanglement, as tracing out either one of the modes would give a thermal statistic for the other. Moreover, it is easy to see that for this state, due to the perfect photon number correlation, the noise reduction factor is $\sigma_{\text{TWB}} = 0$.

In Fig. 4(a), the uncertainty $\Delta\tau$ on the estimation is plotted against the parameter τ in the case of each of the states discussed. The curves are obtained by simply substituting the Fano factor of the different states considered in Eq. (9), for the direct scheme, and $\sigma = 0$ in (13) for the correlated case. The minimum uncertainty attainable in the estimation of a BS parameter[39] is reached, for every value of τ by both the TWB and the Fock state. It is not surprising that the Fock state reaches the lower bound to the uncertainty, since the estimation is based on photon number measurement, for which this state has no noise. When lossless channels are considered, the use of quantum correlations allows to erase the quantum noise present in the probe beam, by exploiting the information on the photon number fluctuation measured in the reference beam, reproducing the situation in which the field is prepared in a Fock state. The coherent state, plotted with a dotted line, is a useful reference for the performance of the TWB state, since as mentioned before, the former represents the SNL and so the limit achievable with classical states. The advantage of TWB over the SNL gets more evident in the region of high τ, corresponding to low deflections. The thermal state is, as expected, the worst one and is reported to show the disadvantage in the use of of light modes in noisier states unless quantum correlations are used.
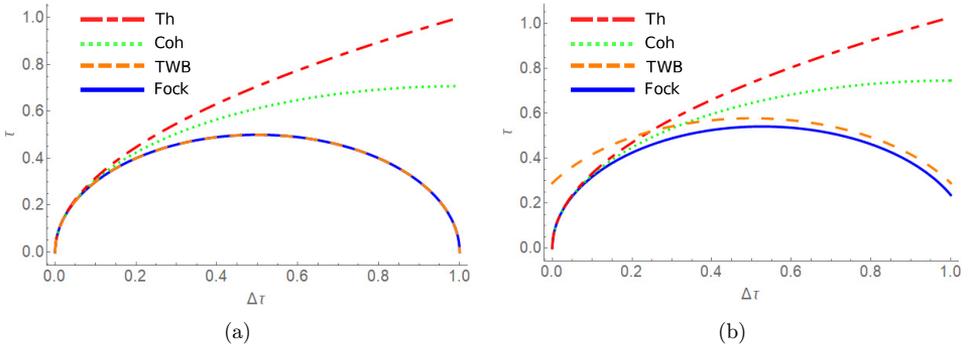
Fig. 4. (a) Uncertainty on the estimation of the BS parameter $0 < \tau < 1$, modeling a beam deflection. Referring to Scheme 3(a) the input states are Fock (solid line), coherent (dotted line) and thermal state (double dashed line). The TWB state result, the dashed line coinciding with the Fock state, refers to Scheme 3(b). (b) Uncertainty on the estimation of the BS parameter $0 < \tau < 1$, modeling a beam deflection, with efficiency $\eta = 0.9$. The uncertainty of the measurement Scheme 3(a) is plotted in the case of optical efficiency $\eta = 0.9$, meaning that a fraction $1 - \eta$ of the initial number of photons are lost. The input states considered are Fock (solid line), coherent (dotted line) and thermal (double dashed line) state. The TWB state result, plotted with the dashed line, refers to Scheme 3(b), where the efficiency is considered $\eta = 0.9$ in both the probe and reference channel.

Up until now, possible photon losses have not been considered, although they are unavoidable in any real optical scheme. Since optical losses are random processes, that add a certain amount of noise, sub-Poissonian behavior and quantum correlations are strongly affected by them. The Fano factor and the NRF measured in case of a fraction $0 \leq 1 - \eta \leq 1$ of photons lost in the channel are

$$F_\eta = \eta F + 1 - \eta, \quad \sigma_\eta = \eta \sigma + 1 - \eta, \tag{15}$$

where for σ_η equal losses on the correlated channels have been assumed.

In Fig. 4(b) the uncertainty is reported in the case of a high, but not perfect, efficiency, $\eta = 0.9$, evaluated by substituting expressions (15) into Eqs. (9) and (13). In this scenario, the performance of the TWB state does not coincide anymore with the one of the Fock states but it becomes slightly worse. An interesting feature is that the uncertainty of the TWB estimation does not approach zero as $\tau \to 0$ and as a consequence, the TWB performs worst than any other configuration in the high deflections region. This is a consequence of the choice of the estimator in Eq. (11), and can be eliminated with a different one. However the advantage of this estimator over other tested estimators, and the reason why it has been chosen here, is that it allows to improve the sensitivity for small deflections, the one we are more interested in. In this region, the TWB state approaches the result of the Fock state, even in the presence of losses, and gives a sensible improvement over the SNL.

Finally, in Fig. 5, we report the maximum value of the detected noise reduction factor, $\sigma_{\max}$, which still provides an advantage over the SNL, i.e. $\Delta\tau_C(\sigma_{\max}) < \Delta\tau_{\mathrm{SNL}}$. It is interesting to notice how, the higher the deflection (smaller
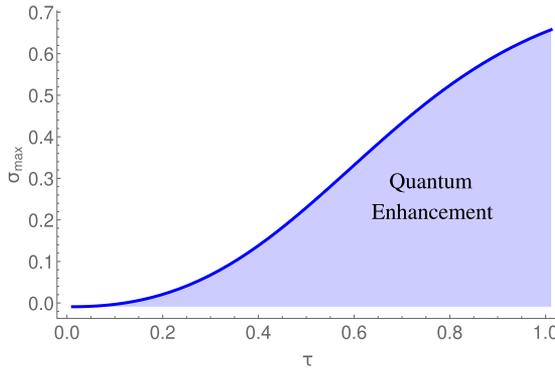
Fig. 5.   *NRF needed to beat the SNL.* The plot represents the maximum value of noise reduction factor σ that a correlated state, used in Scheme 3(b), can have in order to have an advantage over the SNL 9.

values of τ), the stronger the correlation has to be to grant an advantage over the classical limit. Moreover even in the limiting case of no deflection, $\tau = 1$, a NRF ≈ 0.7 is still required, a value well below the limit achievable by classical correlations $\sigma_{\text{class}} \geq 1$.

4. Conclusions

In this work, a simple quantum model describing the measurement of a refractive profile, based on the change of the intensity distribution of a beam after the interaction with a sample, has been elaborated to investigate a possible quantum enhancement in the sensitivity. The deflection caused on a single mode of the spatially multimode beam interacting with the test object were modeled using a BS transformation with transmission coefficient τ, where the angle of deflection α is proportional to $1 - \tau$. A direct measurement scheme was compared to one based on the use of quantum correlations. In particular, we found that the TWB state, a state characterized by entanglement in photon number between pairs of spatio-temporal modes, overcomes the SNL both in the ideal lossless case, reported in Fig. 4(a) and in the presence of losses, shown in Fig. 4(b). Moreover, we have shown that only a correlation level well above the classical bound (noise reduction factor $\sigma_{\text{max}} < 0.7$) allows to overcome the SNL, as reported in Fig. 5.

There results show the possibility to reach a quantum enhancement for wide field imaging of refractive profiles inducing an intensity perturbation in the near field, using a TWB configuration. The analysis performed in this work is meant to be followed by a wide field experimental realization of the correlation based scheme with the TWB state. Twin beams are, in fact, currently routinely generated in quantum optics laboratories, and they have already been used for sub-shot noise imaging of absorption profiles. Thus, the scheme suggested in this work for refractive profile measurements is feasible with the current technology.

Realizing sub-SNL wide field imaging is especially important when there is a limit on the energy that can be used to probe samples. For this reason, sub-SNL imaging of refractive profiles would have useful application, for example, in the analysis of quasi transparent biological sample, giving complementary information to the one obtained using other measurements.

Acknowledgments

References

1. M. Genovese, *J. Opt.* **18** (2016) 073002.
2. I. R. Berchera and I. P. Degiovanni, *Metrologia* **56** (2019) 024001.
3. G. B. Lemos, V. Borish, G. D. Cole, S. Ramelow, R. Lapkiewicz and A. Zeilinger, *Nature* **512** (2014) 409 EP.
4. E. D. Lopaeva, I. Ruo Berchera, I. P. Degiovanni, S. Olivares, G. Brida and M. Genovese, *Phys. Rev. Lett.* **110** (2013) 153603.
5. Z. Zhang, S. Mouradian, F. N. C. Wong and J. H. Shapiro, *Phys. Rev. Lett.* **114** (2015) 110506.
6. Y. Zhang, D. England, A. Nomerotski, P. Svihra, S. Ferrante, P. Hockett and B. Sussman, Multidimensional quantum illumination via direct measurement of spectro-temporal correlations (2019).
7. D. Gatto Monticone, K. Katamadze, P. Traina, E. Moreva, J. Forneris, I. Ruo-Berchera, P. Olivero, I. P. Degiovanni, G. Brida and M. Genovese, *Phys. Rev. Lett.* **113** (2014) 143602.
8. A. Classen, J. von Zanthier, M. O. Scully and G. S. Agarwal, *Optica* **4** (2017) 580.
9. T. B. Pittman, Y. H. Shih, D. V. Strekalov and A. V. Sergienko, *Phys. Rev. A* **52** (1995) R3429.
10. E. Puddu, A. Allevi, A. Andreoni and M. Bondani, *Opt. Lett.* **30** (2005) 1294.
11. R. Meyers, K. S. Deacon and Y. Shih, *Phys. Rev. A* **77** (2008) 041801.
12. M. Bina, D. Magatti, M. Molteni, A. Gatti, L. A. Lugiato and F. Ferri, *Phys. Rev. Lett.* **110** (2013) 083901.
13. G. Brida, M. V. Chekhova, G. A. Fornaro, M. Genovese, E. D. Lopaeva and I. R. Berchera, *Phys. Rev. A* **83** (2011) 063807.
14. A. Meda, A. Caprile, A. Avella, I. Ruo Berchera, I. P. Degiovanni, A. Magni and M. Genovese, *Appl. Phys. Lett.* **106** (2015) 262405.
15. J. Aasi *et al.*, *Nature Photonics* **7** (2013) 613 EP.
16. I. Ruo Berchera, I. P. Degiovanni, S. Olivares and M. Genovese, *Phys. Rev. Lett.* **110** (2013) 213601.
17. S. T. Pradyumna, E. Losero, I. Ruo-Berchera, P. Traina, M. Zucco, C. S. Jacobsen, U. L. Andersen, I. P. Degiovanni, M. Genovese and T. Gehring, Quantum-enhanced correlated interferometry for fundamental physics tests (2018).

18. C. Schäfermeier, M. Ježek, L. S. Madsen, T. Gehring and U. L. Andersen, *Optica* **5** (2018) 60.
19. A. Meda, E. Losero, N. Samantaray, F. Scafirimuto, S. Pradyumna, A. Avella, I. Ruo-Berchera and M. Genovese, *J. Optics* **19** (2017) 094002.
20. E. Knyazev, F. Y. Khalili and M. V. Chekhova, *Opt. Express* **27** (2019) 7868.
21. J. Sabines-Chesterking, A. R. McMillan, P. A. Moreau, S. K. Joshi, S. Knauer, E. Johnston, J. G. Rarity and J. C. F. Matthews, *Opt. Express* **27** (2019) 30810.
22. V. Giovannetti, S. Lloyd and L. Maccone, *Science* **306** (2004) 1330.
23. V. Giovannetti, S. Lloyd and L. Maccone, *Nature Photonics* **5** (2011) 222 EP. Review Article.
24. M. A. Taylor and W. P. Bowen, *Physics Reports* **615** (2016) 1, Quantum metrology and its application in biology.
25. R. Demkowicz-Dobrzanski, M. Jarzyna and J. Kolodynski, *Prog. Opt.* **60** (2015) 345.
26. R. Schnabel, *Phys. Rep.* **684** (2017) 1, Squeezed states of light and their applications in laser interferometers.
27. S. Barnett, C. Fabre and A. Maıtre, *Eur. Phys. J. D - At. Mole. Opt. Plasma Phys.* **22** (2003) 513.
28. R. C. Pooser and B. Lawrie, *Optica* **2** (2015) 393.
29. N. Treps, N. Grosse, W. P. Bowen, C. Fabre, H.-A. Bachor and P. K. Lam, *Science* **301** (2003) 940.
30. M. A. Taylor, J. Janousek, V. Daria, J. Knittel, B. Hage, H.-A. Bachor and W. P. Bowen, *Nature Photonics* **7** (2013) 229.
31. G. Brida, M. Genovese and I. Ruo Berchera, *Nature Photonics* **4** (2010) 227.
32. N. Samantaray, I. Ruo-Berchera, A. Meda and M. Genovese, *Light: Sci. Appl.* **6** (2017) e17005 EP.
33. D. C. Burnham and D. L. Weinberg, *Phys. Rev. Lett.* **25** (1970) 84.
34. E. Jakeman and J. Rarity, *Opt. Commun.* **59** (1986) 219.
35. Q. Glorieux, L. Guidoni, S. Guibal, J.-P. Likforman and T. Coudreau, *Phys. Rev. A* **84** (2011) 053826.
36. R. C. Pooser and B. Lawrie, *ACS Photonics* **3** (2016) 8.
37. E. Marchand, *Gradient Index Optics* (Academic Press, 1978).
38. G. Settles, *Schlieren and Shadowgraph Techniques* (Springer, 2006).
39. A. Monras and M. G. A. Paris, *Phys. Rev. Lett.* **98** (2007) 160401.
40. E. Losero, I. Ruo-Berchera, A. Meda, A. Avella and M. Genovese, *Scientific Reports* **8** (2018) 7431.
41. U. Fano, *Phys. Rev.* **72** (1947) 26.
42. L. Mandel and E. Wolf, *Optical Coherence and Quantum Optics* (Cambridge University Press, 1995).
43. M. O. Scully, *Quantum Optics* (Cambridge University Press, 1997).